Influence of Indian Ocean SSTs on the East African Short Rains

Weiran Liu (wrliu@utexas.edu), Kerry H. Cook, and Edward K. Vizy

Jackson School of Geosciences, The University of Texas at Austin

Introduction

Precipitation over tropical East Africa (EA) exhibits pronounced regional variation and complicated seasonality. Past studies link variability in the short rains (during boreal fall) with SST variability in the Indian Ocean (IO), but there are unsolved questions. For example, which region (or regions) of the IO dominate in influencing the EA short rains, or is the impact from basin-wide SSTs?

The purpose of this study is to determine the regionality of the Indian Ocean SST forcing and EA precipitation responses, and to identify the relevant mechanisms. We identify hot spots of influential SSTAs, and study the hydrodynamics of the resulting perturbations in isolation and combined.

Methodology

- The WRF regional model (3.8.1) is run at 30-km horizontal resolution with 40 vertical levels and a model time step of 60 seconds to produce **five 20-year (1998-2017) ensembles** representing a control climate and idealized SSTA simulations (Table 1). Each ensemble member is initialized on August 1 of a different year (1998-2017) and run to December 31.

- Initial, lateral, and surface boundary conditions are specified at 6-hourly intervals from the ERAI reanalysis for each year (1998-2017). CTL uses climatological ERAI SSTs (Fig. 1b) except for Lake Victoria where Operational Sea Surface Temperature and Sea Ice Analysis (OSTIA) SSTs averaged from 2012 to 2017 are used.

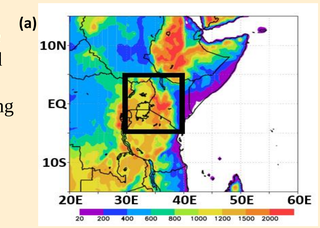

Fig 1. (a) EA analysis domain (black box) with elevation (m). (b) SSTs in CTL (shaded) and SSTAs superimposed in the perturbation simulations (contours). Unit: K.

Table 1. Ensemble descriptions

Ensemble name	Imposed SSTA
Control (CTL)	None
Western IO (WIO)	SSTA1
Central IO (CIO)	SSTA2
Eastern IO (EIO)	SSTA3
Warm-cold IO (ALL)	SSTA1, SSTA2, and SSTA3

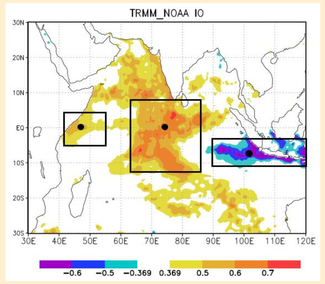

Fig 2. Correlations of TRMM rainfall averaged over the EA analysis domain (Fig.1a) and NOAA OI SSTs averaged Oct 1 to Dec15 for 1998-2017. Only correlations with confidence levels higher than 90% are shaded.

- **SSTA regions shown in the Fig. 1b are chosen according to observed correlations of EA short rains and IO SSTs (Fig. 2).**

- EA short rains are positively correlated to western and central IO SSTs, and negatively correlated to eastern IO SSTs.
- Correlations among the SSTAs averaged over the three black boxes shown in Fig. 2 are calculated. SSTAs in western and central IO are highly correlated while western and eastern IO SSTAs are not significantly correlated at the 90% confidence level.

Model Evaluation

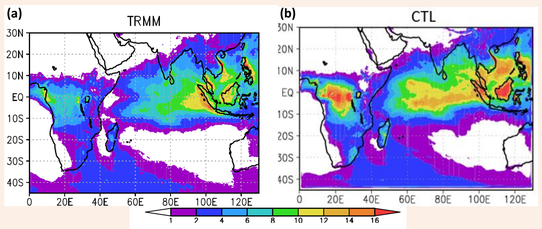

Fig 3. Climatological (1998-2017) precipitation averaged over Oct 1-Dec 15 in (a) TRMM and (b) the CTL ensemble. Unit: mm/day.

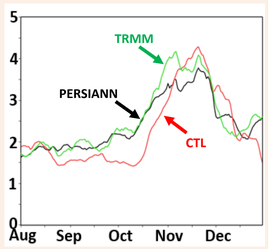

Fig 4. Daily precipitation smoothed using an 11-day running mean averaged over the EA region in PERSIANN (black), TRMM (green), and CTL (red). Unit: mm/day.

- **CTL reasonably captures the distribution and seasonality of precipitation as observed in TRMM and PERSIANN. There is a wet bias over other regions including the Congo Basin.**
- **CTL captures the regional circulation in ERAI and JRA-55 accurately (not shown).**

Results

Moisture budget analysis of EA short rains in CTL

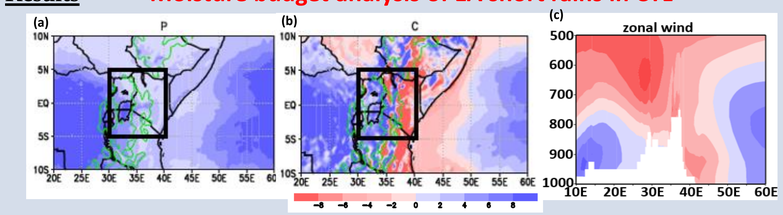

Fig 5. (a) P and (b) C terms in the moisture budget averaged over Oct 1-Dec 15 in CTL. Units: mm/day. Green contours are elevations of 1300 m. Black box shows the EA analysis domain.
(c) Zonal wind along the equator from 1000 to 500 hPa (Oct 1-Dec 15) in CTL. Units: m/s.

$$\bar{P} = \bar{E} - \overline{\int_0^{p_s} \left[\nabla \cdot (q\,\vec{V} + \frac{\partial q}{\partial t})\right] \frac{dp}{g\rho_w}} \qquad \bar{P} = \bar{C} + \bar{A} + \bar{O} + \bar{T} + \bar{E},$$

$$\bar{C} = -\frac{1}{g\rho_w}\sum_0^{p_s} \bar{q}(\nabla_h \cdot \vec{V})\,dp \qquad \bar{A} = -\frac{1}{g\rho_w}\sum_0^{p_s} (\vec{V} \cdot \nabla_h\, q)\,dp$$

$$\bar{O} = -\frac{1}{g\rho_w}\overline{(q\omega)}_s \approx -q_s\vec{V}_s \cdot \nabla p_s \qquad \bar{T} = -\frac{1}{g\rho_w}\nabla_h \cdot \left[\int_0^{p_s} (\overline{q\,\vec{V}} - \bar{q}\,\bar{\vec{V}})dp\right]$$

P: precipitation
C: convergence
O: orographic precipitation
A: advection
T: transient
E: evapotranspiration

- **The simulated processes that support regional rainfall as revealed by the atmospheric moisture budget agree well with reanalyses (not shown).**

- **The mechanisms that support precipitation in the western and eastern parts of the equatorial EA analysis domain are fundamentally different due to the presence of complex topography. The short rains over the western half of the domain are mainly supported by wind convergence in a moist environment, while orographic uplift plays a dominant role farther east.**

Precipitation and circulation anomalies in the perturbation simulations

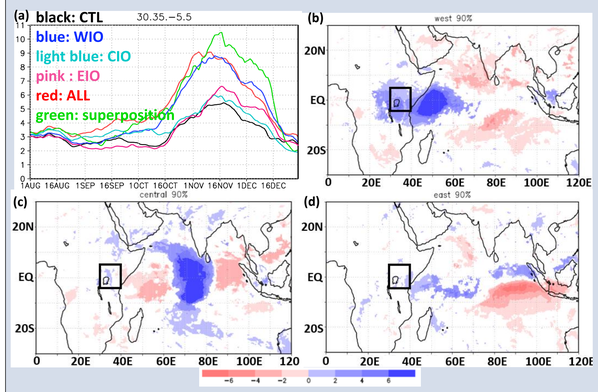

Fig 6. (a) 11-day running mean of precipitation (30-35E, 5S-5N) in CTL (black), WIO (dark blue), CIO (light blue), EIO (pink), ALL (red), and the superposition of the WIO, CIO, and EIO ensembles (green). Anomalous precipitation for the (b) WIO, (c) CIO, and (d) EIO simulations averaged over Oct 1- Dec 15. Units: mm/day.

- **Warm western IO SSTAs are associated with significantly increased short rains over 95% of the EA analysis domain. Central IO SSTAs result in wetter conditions in the western EA analysis domain (29% coverage) and drier conditions in the east (8% coverage). Eastern IO SSTAs enhance precipitation over 30% of the EA analysis domain. The maximum precipitation anomaly associated with western IO SSTAs is about three times larger than the anomalies due to central and eastern SSTAs in the simulation.**
- **The response of EA precipitation to the three SSTAs together (ALL ensemble; Table 1) does not equal the sum of the responses to the SSTAs individually. The western IO SSTA dominates the anomalous EA precipitation when the three SSTAs occur at the same time.**

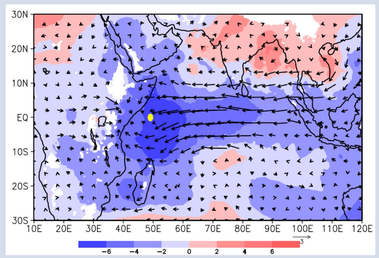

Fig 7. Anomalous geopotential heights (shaded; gpm) and winds (vectors; m s-1) at 850 hPa in the WIO ensemble averaged over Oct 1 – Dec 15. The yellow dot shows the location of the maximum of SSTAs in the WIO simulations.

- **Geopotential height anomalies and wind anomalies in the WIO ensembles are similar to the response to steady thermal forcing on the equator from the shallow water equations (Gill 1980). The equatorial zonal flow to the west of the heating is weaker than to the east, different from the classic Gill type response (1980), possibly due to the influence of the highlands over East Africa and Ethiopia (up to 700 hPa).**

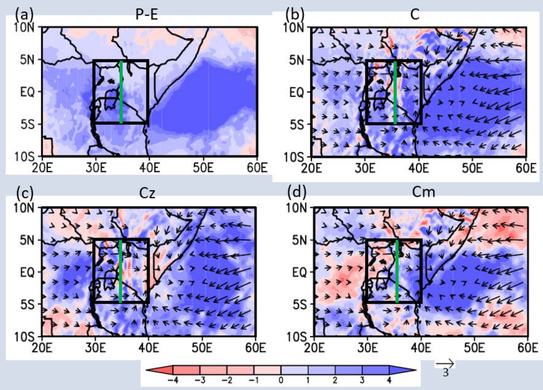

Fig 8. Anomalous (a) precipitation minus evapotranspiration, (b) moisture convergence term, (c) zonal moisture convergences term, and (d) meridional moisture convergence term in the moisture budget for the WIO ensemble climatology. Unit: mm/day. Vectors in (b)-(d) are anomalous winds (m s-1) at 850 hPa for the WIO ensemble climatology. Black boxes denote the full EA analysis domain. Green lines are the boundaries between western and eastern EA analysis domain.

- **The anomalous C term resembles the P-E anomaly in the WIO simulations. The C term is also the largest contributor in the other ensembles (not shown). Increased P-E over the western EA analysis domain is associated with zonal moisture convergence, while it is more closely associated with meridional moisture convergence over the eastern EA.**
- **The positive meridional moisture convergence anomalies over the coast (Fig. 8d) are associated with the cyclonic anomaly over (35°-55°E, 0°-15°S) and meridional wind perturbations over (40°-50°E, 0°-15°N) in the presence of the Rossby mode (Fig. 7).**

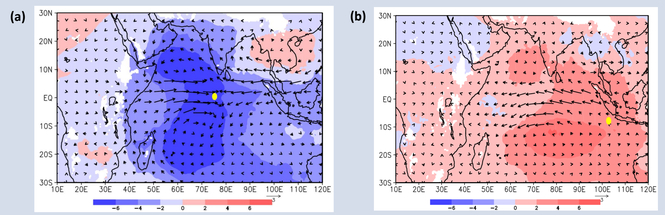

Fig 9. Anomalous geopotential heights (shaded; gpm) and winds (vectors; m s-1) at 850 hPa averaged over October 1 – December 15 in the (a) CIO and (b) EIO ensembles. The yellow dot shows the location of the maximum of SSTAs. Topography is masked out.

- **The anomalous equatorial zonal flows in the CIO simulations are associated with anomalous zonal wind convergence in the moist environment over the central Indian Ocean (not shown) and, therefore, the significantly-increased precipitation (Fig. 6b).**
- **The anomalous low-level height response in the EIO simulations is asymmetric about the equator as the center of the SSTAs is located more off the equator (10°S) compared to the WIO and CIO cases.**

Conclusions

1. The EA short rains are positively correlated with SSTAs in the western and central IO, and negatively correlated with eastern IO SSTAs. While SSTAs in the western and central IO are highly correlated with each other, eastern IO SSTAs vary independently on interannual time scales.

2. SSTAs in the western IO exert a stronger influence on the equatorial EA short rains than central and eastern SSTAs in terms of both the coverage of significantly-changed precipitation and the magnitude of the precipitation response. Warm western IO SSTAs are associated with significantly increased short rains over 95% of the EA analysis domain, while only about 30% of the EA analysis domain responds to central and eastern IO SSTAs.

3. Responses in the western and eastern parts of the equatorial EA domain are fundamentally different due to the region's complex topography.

4. **The atmospheric moisture budget analysis shows that the anomalous wind convergence closely resembles the precipitation anomaly in all cases.** The patterns of geopotential heights and winds anomalies caused by positive western and central IO SSTAs are similar to the Gill-type response (1980) to steady heating on the equator, while the simulations with negative eastern IO SSTAs are similar to the off-equator cooling case. The main differences between the classic Gill response (1980) and our cases are due to the presence of complex topography and background flows.

Acknowledgements This work was funded by **National Science Foundation Award # 1356386**. The Texas Advanced Computing Center (TACC) at the University of Texas at Austin provided the high performance computing and database resources for the simulations.